



CFD: Progress and problems

Steven A. Orszag^{a,b,*}, I. Staroselsky^b

^a *Department of Mathematics, Yale University, New Haven, CT 06520-8283, USA*

^b *Cambridge Hydrodynamics, Inc., P.O. Box 1403, Princeton, NJ 08542, USA*

Abstract

We give a brief review of the state-of-the-art in computational fluid dynamics. Most of this paper concerns several flow examples that emphasize the physics, mathematics, and numerics of the flows being simulated. © 2000 Published by Elsevier Science B.V. All rights reserved.

PACS: 02.30.J; 02.60; 47.11; 47.27

Keywords: Computational fluid dynamics; Large-eddy simulation; Very large-eddy simulation; Burgers equation; Turbulence; Numerical methods

This paper summarizes some of the issues discussed by us at the American Physical Society's (APS) Centennial Symposium held this year. While the history of computational fluid dynamics (CFD) is substantially briefer than that of the APS, there has been much superb work and progress made using CFD over the past half century. This work has led to significantly new physical insights into the behavior of flows ranging from laminar to turbulent, from nonreacting to reacting, from Newtonian to non-Newtonian, Indeed, there is much technology now available to reliably compute flows in complex geometries with complex physics. Computation now stands as an equal partner with mathematical analysis and experimental inquiry. CFD has become such an effective tool that many of our colleagues who previously would rely only on experiment to uncover fluid phenomena now use CFD to achieve their goals more rapidly and cost effectively.

The state-of-the-art of computation has advanced on many fronts. On the one hand, computer hardware itself has improved dramatically over the last half century. As we close the 20th century, computers are 10^9 times faster and more cost effective than they were in the days of World War II. Indeed, Moore's law that asserts computer speedups by a factor 2 every 1.5–2 years fits well with this remarkable performance achievement. Furthermore, while state-of-the-art electronic chip manufacturing today uses $0.25\ \mu$ feature size technology, the path to $0.05\ \mu$ or smaller technology now seems apparent, thereby ensuring Moore's law-like speedups for the next 15 years or so. The resulting three order-of-magnitude increase of computer capability in this relatively short future time span will clearly open new vistas for CFD.

The impressive performance improvements in computers have been matched by developments in numerical and mathematical technologies for solving problems. As computation opens new application areas, so too does it stimulate new ideas for mathematical and physical modeling and algorithms. Recent ad-

* Corresponding author. E-mail: sao@xi.com.

vances enabled by fast transform methods, fast multipole methods, and the like allow solution of problems using $O(1)$ arithmetic operations per degree-of-freedom (DOF) used to represent the field (perhaps corrected by logarithmic factors of the total number of DOFs). In contrast, classical algorithms are often much slower (e.g., Gauss elimination solution of a dense linear system with N unknowns requires $O(N^2)$ operations per DOF). The natural question to ask is where future algorithms and advances are likely to arise, since they are not likely to reduce the number of operations to fewer than $O(1)$ operations per DOF. The answer has become increasingly clear in recent times, viz., techniques are being developed now to enable marked reduction in the number of DOFs needed to represent a complex field. Such techniques include, but are not limited to, wavelet methods, adaptive gridding methods, complex analysis, and the like.

Another critical area for the development of CFD is that of physical modeling. The need for physical modeling is most apparent in turbulent flows which occur at high Reynolds numbers R defined as VL/ν where V and L stand for the characteristic flow velocity/length scale and ν is the typical value of viscosity or any kinematic transport coefficient. It is well known that, on the basis of Kolmogorov theory of turbulence, a flow at Reynolds number R engages roughly $O(R^{9/4})$ spatial DOFs with roughly $O(R^{1/2})$ temporal DOFs. Since real-world applications (including aircraft and ships) occur at $R = O(10^8-10^9)$, the total number of DOFs involved can be in excess of 10^{24} (i.e. comparable to the Avogadro's number). Such problems are well beyond foreseeable computer power so that their solution requires elimination of DOFs to reduce the effective problem size.

There are several general methods of doing this, including large eddy simulations (LES), very large eddy simulations (VLES) and analytical theories of turbulence. This classification is based on the number of DOFs removed from the dynamics. In LES, all DOFs smaller than the filter scale Δ (roughly, the grid size) are modeled while all DOFs larger than Δ are computed via a modified set of Navier–Stokes equations. Models for the DOFs representing small scales are based on universal properties of fully developed turbulence and range from the so-called Smagorinsky model to renormalized scalar viscosity formulations to

tensor viscosity formulations. An outstanding physics issue is to find a good representation of the much less universal turbulent flow near walls. Lacking this, current LES simulations are typically limited to R 's which are barely a factor of 2 larger than those achievable by full Navier–Stokes simulations. The other issues in present-day LES include independence of the results on the filter/grid size and the inclusion of complex physics.

In VLES, scales within the Kolmogorov inertial and dissipation range are modeled while larger-scale “coherent” eddies are computed explicitly. Such models are related to classical Reynolds averaging but recent results based on renormalization group techniques demonstrate the key role played by coherent eddies, time dependence, and transitional effects in a number of flows. Successes of this new approach are reported elsewhere [1,2]. The difference between VLES and LES is that, in the former, only the large, anisotropic eddies beyond the Kolmogorov inertial range are resolved numerically. An elementary argument may be used to estimate which eddies are resolved by VLES and which eddies are modeled. In the Kolmogorov theory, the local velocity of an inertial range eddy of size h is proportional to $\mathcal{E}^{1/3}h^{1/3}$, where \mathcal{E} is the rate of energy dissipation (per unit mass). Therefore, the characteristic time-scale of this eddy is of order $\tau_h = h^{2/3}\mathcal{E}^{-1/3}$. Large, anisotropic eddies are characterized by the time scale $\tau_S = 1/|S|$ where S is the local rate-of-strain. The coherent large-scale, anisotropic eddies are characterized by $\tau_S \ll \mathcal{O}(\tau_h)$ or $h > \mathcal{O}(\mathcal{E}^{1/2}/|S|^{3/2})$.

Finally, analytical theories use field theoretical techniques to model all DOFs of turbulence. Such theories, especially Kraichnan's DIA theories, have gone far to elucidate fundamental turbulence processes but, unfortunately, remain difficult to compute for complex shear flows.

In the remainder of this paper we give three case studies which highlight the need for care in CFD analysis. The relative simplicity of these flow problems uncovers the necessity to understand the physics and mathematics/numerics of the underlying problem in order to make progress and that brute force computing power is not always sufficient. This is especially true for the more complex research and engineering flows encountered in modern CFD applications.

1. Example 1: Steady state solution of Burgers’ equation

Here we present a numerical study of one-dimensional shock wave propagation governed by Burgers’ equation

$$\frac{\partial u}{\partial t} + u \frac{\partial u}{\partial x} = \nu \frac{\partial^2 u}{\partial x^2} \tag{1}$$

in the $x - t$ domain $[-1; 1] \times \mathbf{R}_+$ with the boundary conditions $u(\mp 1, t) = \pm 1$. A steady solution is achieved as $t \rightarrow \infty$ that is antisymmetric in x and for small viscosity $\nu \ll \ll 1$ represents a “shock wave” of width $O(\nu)$ located at $x = 0$,

$$u(x, \infty) = -\tanh(x/2\nu) / \tanh(1/2\nu). \tag{2}$$

As a test, we solve (1) with an initial condition corresponding to a shock wave centered at $x_0 \neq 0$ and width $\Delta \neq 2\nu$:

$$u(x, 0) = a \tanh((x - x_0)/\Delta) + b \tag{3}$$

with a, b chosen so that the boundary condition $u(\mp 1, t) = \pm 1$ are satisfied.

The results presented below are obtained using a centered second-order finite difference code with explicit time stepping. In Fig. 1 we plot the solution of the initial-value problem for $\nu = 0.03$, $\Delta = 0.1$, and $x_0 = -0.8$. Grid resolution is chosen so that errors are small (of the order of width of the plotted curve).

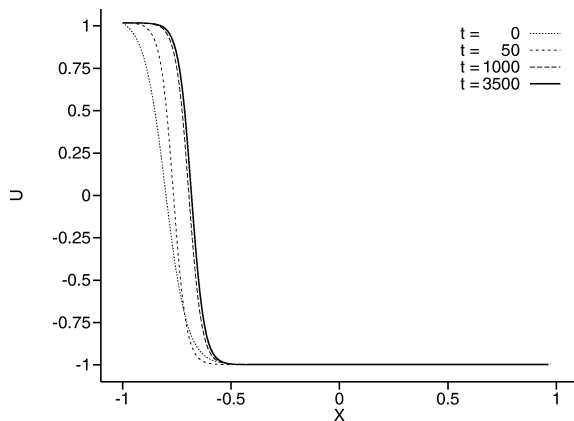


Fig. 1. Numerical solution of the Burgers’ equation at $t = 0, 50, 1000, 3500$, from left to right, respectively. The exact asymptotic steady state solution is a shock of the same shape located at $x = 0$ (not shown here).

Qualitatively, the solution quickly acquires a reasonable profile, having the spatial structure of (2), and starts moving to the right towards the true equilibrium shock location of $x_{\text{center}} = 0$; here x_{center} is defined by $u(x_{\text{center}}, t) = 0$. The movement of x_{center} , however, is quite slow and stagnates at times $O(1000)$. This is especially clear from Fig. 2 where we plot x_{center} as a function of time. Without knowing the exact analytical solution (2) which of course corresponds to $x_{\text{center}} = 0$, one could easily conclude from Figs. 1 and 2 that the steady state solution of (1) is faithfully obtained at $t = O(10^3)$ and corresponds to $x_{\text{center}} = -0.742$. Note, that these computational times of 50, 1000, and 3500+ are indeed large compared to both the advection time (of the order of $L/u \approx 1$) and the diffusion time (of the order of $L^2/\nu \approx 30$).

From the formal point of view, the slow numerical convergence in the above example is due to the fact that, for each intermediate time, the nonlinear term on the left side of (1) vanishes almost everywhere in the domain except for a narrow strip of the order of $\nu \ll \ll 1$. That leaves it to the viscous (Laplacian) term to drive the solution to the exact steady state; this is of course anomalously slow when the viscosity is small. Indeed, the full numerical solution of (1) with (3) with our choice of boundary conditions and

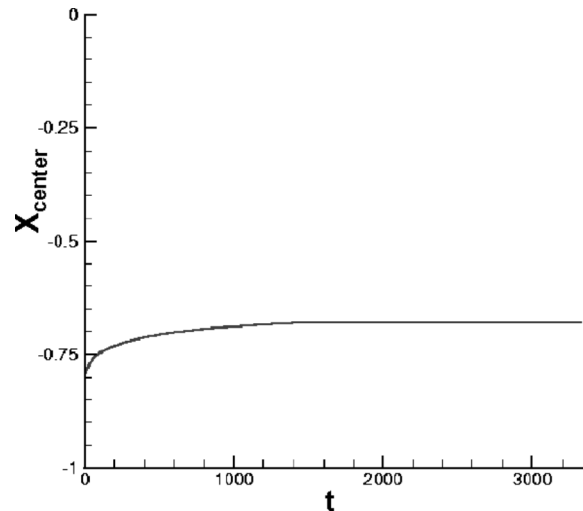


Fig. 2. Location of the shock in the numerical solution of the Burgers’ equation as a function of time. This location $x_{\text{center}}(t)$ is defined by $u(x_{\text{center}}, t) = 0$.

parameters requires $t = O(10^{12})$ to reach the steady state (2).

Actually, the effect of nonlinearity cancellation has deep physical origins and is quite generic. To see this, we consider the case of high Reynolds number incompressible flow problem in two dimensions.

Let us recall that the Navier–Stokes equations may be recast as the vorticity equation

$$\frac{\partial \omega}{\partial t} + e_{ab} \frac{\partial \omega}{\partial x_a} \frac{\partial \psi}{\partial x_b} = \nu \Delta \omega \quad (4)$$

where the antisymmetric tensor $e_{ab} : e_{12} = -e_{21} = 1; e_{11} = e_{22} = 0$ is introduced and the vorticity, ω , and the stream function, ψ , are related to the velocity field and to each other via

$$v_a = e_{ab} \frac{\partial \psi}{\partial x_b}; \quad \omega = e_{ab} \frac{\partial v_a}{\partial x_b} = -\Delta \psi.$$

When the viscosity ν is small compared to V and L ($Re \equiv VL/\nu \gg 1$), the viscous term on the right side of (4) is non-negligible compared to the nonlinear term on the left side only in narrow boundary layers of the width of $\delta = f(Re)L \ll \ll L$, with the function f usually involving negative powers of Re . In the remainder of the domain, there is a continuum of solutions in which (4) is satisfied as a quasi-steady state. Indeed, for each single-valued function F , “Batchelor” eddies in which $\omega \approx F(\psi)$ nearly cancel the nonlinearity in (4):

$$e_{ab} \frac{\partial \omega}{\partial x_a} \frac{\partial \psi}{\partial x_b} \frac{dF(\psi)}{d\psi} \approx e_{ab} \frac{\partial \omega}{\partial x_a} \frac{\partial \omega}{\partial x_b} \equiv 0.$$

There is, of course, only one such bulk solution which matches the wall boundary conditions via the boundary layer behavior in the strip of the width δ . This solution requires long viscous-like times to be achieved while Batchelor eddy states are achieved on convective time scales.

The analogy with the above example of the Burgers equation is clear. At large enough resolution, one may observe steady convergence of the computational problem to a solution corresponding to some function F which would seem to remain steady at all practically achievable simulation times. The boundary condition information propagates anomalously slowly to the bulk of the domain though the boundary layer when the Reynolds number is large.

2. Example 2: Unsteady turbulent flow past a compressor blade’s trailing edge

Here we describe some of our recent results on flow past a compressor trailing edge which indicate that steady-state Reynolds-averaged computations prove inadequate in flows with large-scale coherent eddies.

The domain geometry is plotted in the lower-right part of Fig. 4. The Reynolds number for this flow is 56 400 based on the diameter of the half-cylinder trailing edge. The inlet, taken at 10.6 diameters upstream, is a symmetrical zero pressure gradient turbulent boundary layer set to match experimental conditions. A number of runs were performed using different turbulence transport models for steady-state and time-dependent cases at different spatial resolutions, and a steady-state case with a splitter plate.

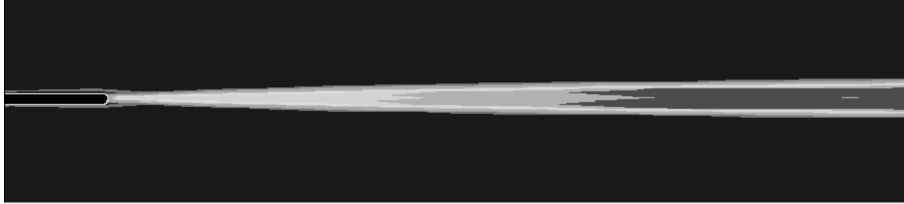
First, steady-state computations of the trailing edge using a standard Reynolds-averaged turbulence transport model with 25 000 grid cells in the domain seem to indicate convergence. The flow fields of pressure and eddy viscosity plotted in Fig. 3 correspond to a residual error in the pressure solver of the order of 5×10^{-5} . These flow fields are symmetric with the pressure distribution showing a large symmetric separated eddy. The steady solution with a splitter plate is very similar.

In principle, this computational study could have been stopped at this point. A reasonable simulation model has provided a reasonably well converged solution of the problem. However, tests with increased resolution in the wake region (with 40 000 cells) show that the residual error in the pressure solver increases by two orders of magnitude to 5×10^{-3} . This error reduces by only about 20% when the grid is further refined uniformly across the domain with about 200 000 points. The ‘steady’ flow fields obtained in these grid-refined cases are not symmetric.

This case study with the steady solver is typical of how non-vanishing residuals can hint at true time dependence in complex flows. In the present case, a time-dependent solution is obtained using the VLES transport model [1,2], which has a higher effective Reynolds number than the standard Reynolds-averaged model.

With the VLES model, the time-dependent large-scale flow is computed with a Strouhal frequency approximately 0.2 in agreement with experiment. In

Effective (Eddy) Viscosity



Pressure



Pressure distribution shows weak, large, symmetric separated eddy

Fig. 3. Distributions of the eddy viscosity and pressure for a flow past compressor trailing edge obtained using a steady Reynolds-averaged flow solver.

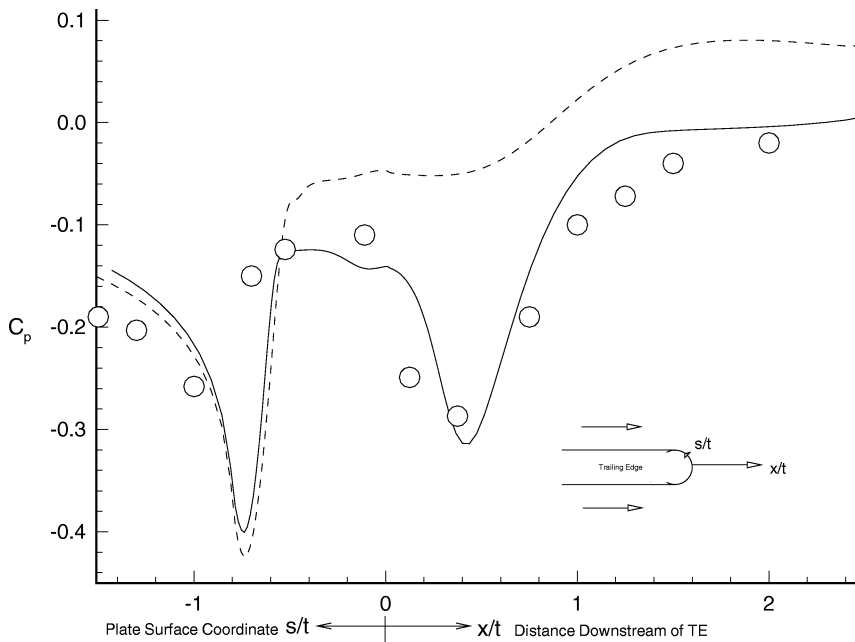


Fig. 4. Pressure coefficient distribution in the flow past compressor trailing edge as a function of the distance downstream of the trailing edge (for $x > 0$) or the plate surface coordinate (for $x \ll 0$). The solid line, corresponding to time averaged VLES results, is in good agreement with the experimentally observed behavior (circles). Results obtained using steady flow solver (dotted line) fail to capture the flow behavior in the wake.

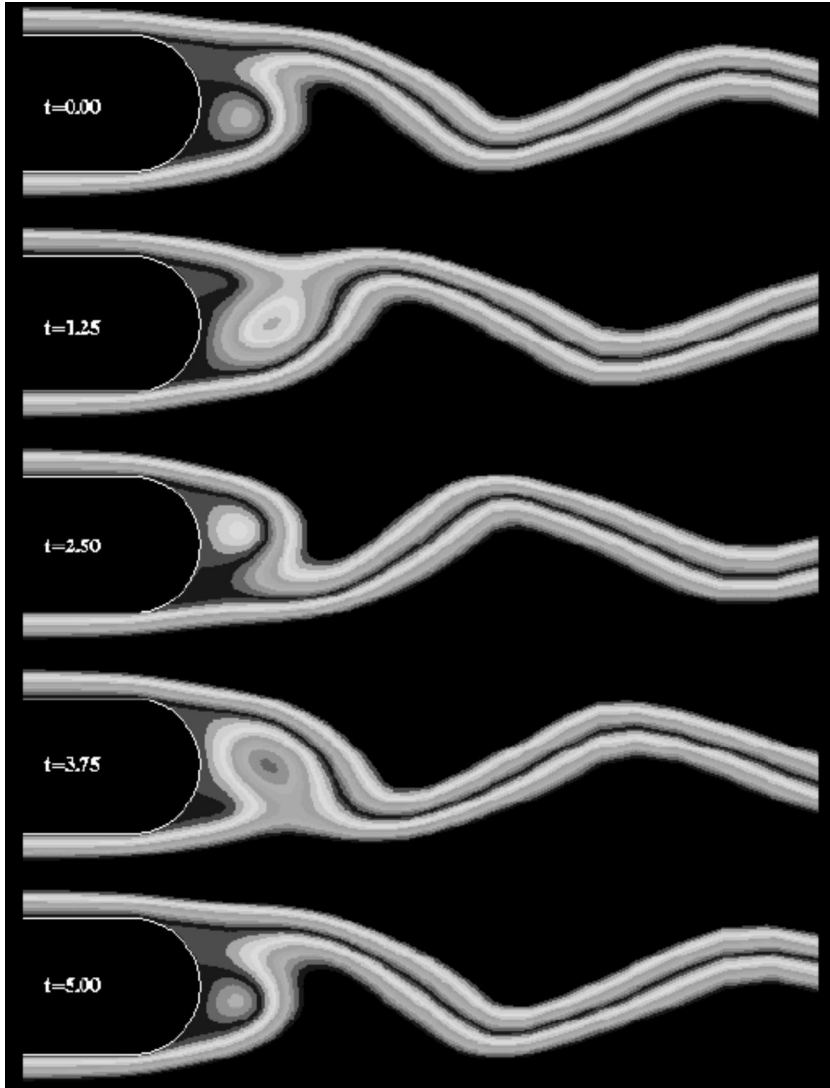


Fig. 5. Vortex evolution in the flow past compressor trailing edge obtained using the time-dependent VLES turbulence model. Plotted are streamlines as a function of time corresponding to $Re = 56400$. The wake eddies are much smaller and stronger than those obtained by the steady Reynolds-averaged flow solver.

Fig. 4 the time-averaged distribution of C_p for the VLES run is plotted. The time-averaged VLES result is also in reasonable agreement with experiment and shows a strong pressure minimum in the wake. In contrast, the steady-state results (with and without a splitter plate) are similar to results obtained by VLES for runs with a splitter plate longer than roughly the diameter of the trailing edge (which are close to

experiment for flow with a splitter plate but not plotted here).

The time-dependent VLES run gives a stronger and smaller vortex. The results plotted in Fig. 5 show that the magnitude and location of the velocity minimum are in reasonable agreement with the experimental values of -0.2 and 0.4 , respectively. It appears that the VLES model, by producing less turbulence as

a result of smaller eddy viscosities, can predict the time-dependent behavior of the (very) largest eddies. This is especially important in computations of three-dimensional effects, e.g., complex flow separation.

3. Example 3: Pressure modes in a cylinder

Consider the problem of finding the axisymmetric modes of pressure within a cylinder:

$$\nabla^2 p = -k^2 p, \quad p = p(r), \quad 0 \leq r \leq 1.$$

The axisymmetric modes satisfy the ordinary differential equation eigenvalue problem

$$\frac{d^2 p}{dr^2} + \frac{1}{r} \frac{dp}{dr} + k^2 p = 0, \quad p(0) \ll \infty, \quad p(1) = 0. \quad (5)$$

It has solutions proportional to the 0th order Bessel function

$$p(r) \propto p(0) J_0(kr),$$

where $k = 2.40483, 5.552008, \dots$ are the zeros of J_0 .

In order to determine this modal spectrum numerically, it may appear best to simplify (5) to remove the first derivative term. By setting $y(r) = \sqrt{r} p(r)$, (5) reduces to the WKB-like problem.

$$\frac{d^2 y}{dr^2} + \left(\frac{1}{r^2} + k^2 \right) y = 0, \quad y(0) = y(1) = 0. \quad (6)$$

Below we list numerical results for the lowest eigenvalue obtained using second-order central differencing for various number of points N (see Table 1).

This very slow convergence is to be compared with much faster converging results for the original, untransformed problem (5) (Table 2).

What is the origin of the astonishingly bad convergence of the transformed problem (5)? The transformation from (5) to (6) is of course exact and is routinely recommended in numerical analysis of second-order differential equations. However, with (6), the relative error in the central differencing scheme is of order 1 near $r = 0$. This becomes clear once we notice

Table 1

N	k	% error	N	k	% error
125	2.6308	9.4	1000	2.5783	7.2
250	2.6101	8.5	5000	2.5518	6.1
500	2.5929	7.8	50000	2.5255	5.0

Table 2

N	k	% error	N	k	% error
10	2.3868	0.75	100	2.4047	0.0075
20	2.4003	0.19	200	2.4048	0.0019
40	2.4037	0.047	1000	2.4048	0.0001

that the asymptotic behavior of the solution of (6) is $y(r) \sim \sqrt{r}$ ($r \rightarrow 0$), while classical differencing formulae assume that Taylor-series analysis holds. Indeed, for (6), it may be shown that the error in k decreases inversely proportional to $\log N$. Thus, increasing the resolution from $N = 10^2$ to $N = 10^{10}$, gives numerical errors in k that decrease only by about a factor of 5 (from roughly 10% to roughly 2%).

Acknowledgments

We would like to acknowledge support by DARPA, ONR, and the NSF. We would also like to thank A. Konstantinov and V. Yakhot for helpful discussions regarding VLES and R. McCrory for introducing us to the peculiarities of Example 3.

References

- [1] S.A. Orszag, I. Staroselsky, W.S. Flannery, Y. Zhang, Introduction to renormalization group modeling of turbulence, in: Simulation and Modeling of Turbulent Flow, T. Gatski, M.Y. Husaini, J. Lumley (Eds.) (Oxford University Press, 1995).
- [2] S.A. Orszag, V. Yakhot, W.S. Flannery, F. Boysan, D. Choudbury, J. Maruzewski, B. Patel, Renormalization group modeling and turbulence simulations, in: Near-Wall Turbulent Flows, R.M.C. So, C.G. Speziale, B.E. Launder (Eds.) (Elsevier Science Publishers, 1993), pp. 1031–1046.